Cross sections for the ^{6}Li(p,^{3}He)^{4}He reaction at energies between 0.1 and 3.0 MeV

A. J. Elwyn, R. E. Holland, C. N. Davids, L. Meyer-Schützmeister, F. P. Mooring, and W. Ray, Jr.
Argonne National Laboratory, Argonne, Illinois 60439
(Received 27 August 1979)

Absolute differential and total (integrated) cross sections for the ^{6}Li(p,^{3}He)^{4}He reaction at proton energies between ~0.14 and 3 MeV are presented, and compared with previous measurements. The results comprise a consistent set of data over much of the energy range of interest to a number of applications. Thermonuclear reaction rate parameters and astrophysical S factors are calculated. The measured angular distributions are compared to predictions of a preliminary R-matrix analysis based on the nuclear properties of energy levels in the mass-7 system.

[NUCLEAR REACTIONS ^{6}Li(p,^{3}He)^{4}He, E_p = 0.14–3 MeV; enriched target; measured $\sigma(E_p,\theta)$, $\sigma(E_p)$; calculated $\langle\sigma v\rangle$, astrophysical S factor.]

I. INTRODUCTION

As part of a continuing program[1,2] to measure absolute reaction cross sections for various light ions with ^{6}Li at energies below a few MeV, we report here the accurate determination of both total and differential cross sections for the ^{6}Li(p,^{3}He)^{4}He reaction at energies between 0.14 and 3.0 MeV.[3] The present data are relevant to the determination of the level structure of ^{7}Be above 5.5-MeV excitation, and taken together with similar data from the ^{6}Li(n,t)^{4}He process, in which the compound nucleus ^{7}Li is formed, is applicable to recent[4,5] multilevel multichannel R-matrix investigations of the nuclear structure in the mass-7 system.

At the same time, the significiance of the ^{6}Li(p,^{3}He) reaction to studies of controlled thermonuclear reactors based on the use of advanced fusion fuels has been discussed by a number of authors.[6] The feasibility for such an application will depend in part on the values of the total reaction cross section at energies below a few MeV. Unfortunately, earlier measurements[7-10] are inconsistent with one another in the range 0.2 to 3 MeV (see Fig. 1). The results reported in the present report serve to clarify the experimental situation at these energies.

The experiment is described in Sec. II and the results including tabulated reaction cross sections are given in Sec. III. Rate parameters, the astrophysical S factor, and some preliminary calculations of cross sections are discussed in the final section.

II. EXPERIMENT

The measurements were performed at the Argonne 4-MV Dynamitron accelerator. The experimental arrangement and procedures have been discussed previously[1] in some detail. Modifications required by the current measurements, as well as a brief review of our techniques, follow below.

The accelerated proton beam entered a 76-cm diam scattering chamber through two defining apertures. The targets placed at the center of the chamber were thin films of LiF enriched to 99.3% in ^{6}Li, evaporated on 10 μg/cm^2 carbon foils. The beam passing through the thin targets was collected in a Faraday cup, in which secondary electron loss was magnetically suppressed, and the total charge was measured with a current integrator. The operation of the integrator was checked by the use of batteries and precision resistors, and found to be accurate to better than 0.5%. For incident proton energies above 0.5 MeV the H_1^+ ion beam from the Dynamitron was used, while at lower energies the H_3^+ molecular ion was selected to give proton energies at the target of $\frac{1}{3}$ of the terminal voltage.

Charged particles in the reaction were detected by collimated Si surface-barrier detectors thick enough to completely stop the reaction products; two were mounted on movable arms within the chamber, while a third fixed at a back angle, served as a monitor in the angular distribution measurements. At energies below 1 MeV, peaks in the pulse-height spectra that correspond to elastically scattered protons or to α particles that arise from the ^{19}F(p, α) reaction (Q = 8.1 MeV) are either too weak or do not interfere at any angle with detection of the ^{3}He and ^{4}He particles of interest. At these energies, therefore, the pulses from the detectors (and associated preamplifiers) were amplified and digitized with 1024-channel analog-to-digital converters interfaced to a PDP 11/45 computer. The data were stored as pulse-height spectra and later transferred to magnetic tape. A typical pulse-height spectrum of the

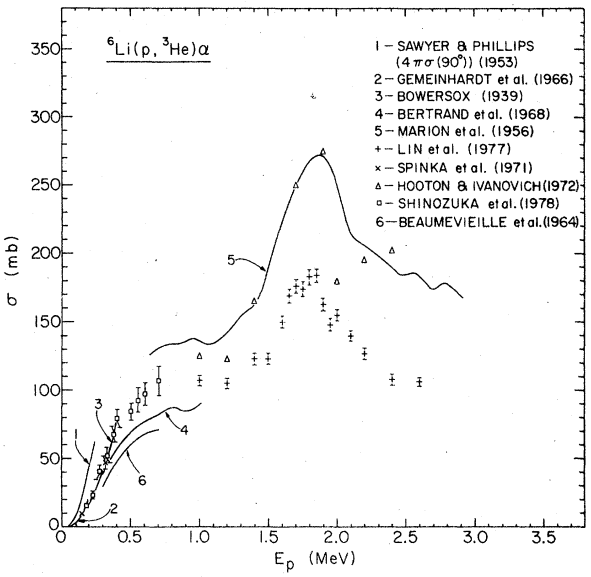

FIG. 1. Previously measured cross sections for the $^6Li(p,^3He)$ reaction at energies below 3 MeV, as given in Refs. 7, 8, 9, and 10.

charged particles from reactions of protons with the ^6LiF targets is shown in Fig. 2.

At energies above 1 MeV, because of interference (at many angles) with both elastically scattered protons and the ^{19}F-reaction α particles, a coincidence method was used. The ^3He and ^4He particle signals from the $^6Li(p,^3He)^4He$ reaction at any forward angle were required to be in time coincidence with the corresponding particle pulses at the kinematically correct backward angle. Pulse-height data from each detector, after passing through spectroscopy amplifiers, were stored both as two-dimensional arrays (256×256 channels) and as separate singles spectra in the computer, and were later output onto magnetic tape. The forward-angle detector subtended a solid angle of 0.21 msr, defining an angular acceptance of somewhat more than 1°. The solid angle of the backward detector was chosen so that both ^3He and ^4He particles coincident with those detected at forward angles could be counted. Singles and coincidence spectra were compared at angles at which the peaks of interest were well separated from the interfering particles mentioned above, and the number of counts always agreed to better than 1%.

Angular distributions were measured at laboratory angles between 35° and 155° at energies up to 1 MeV, and from 20° (or 25° in some cases) to 90° in the higher energy region. By determining the yields of both the ^3He and ^4He particles at each angle, and converting the ^4He values to those for

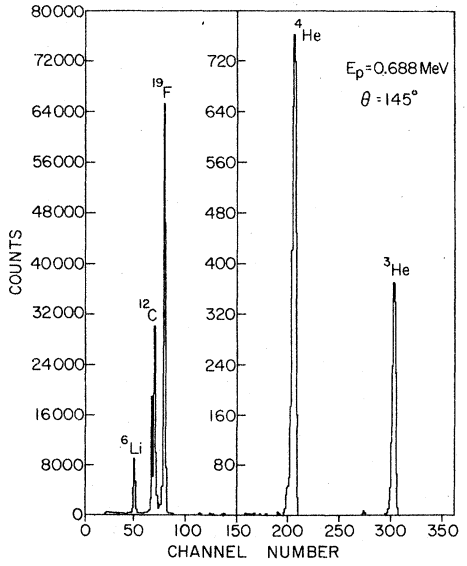

FIG. 2. A typical pulse-height spectrum of charged particles from reactions of protons with ^6LiF on C backings. The peaks labeled ^3He and ^4He are from the $^6Li(p,^3He)^4He$ reaction, while the others represent elastically scattered protons.

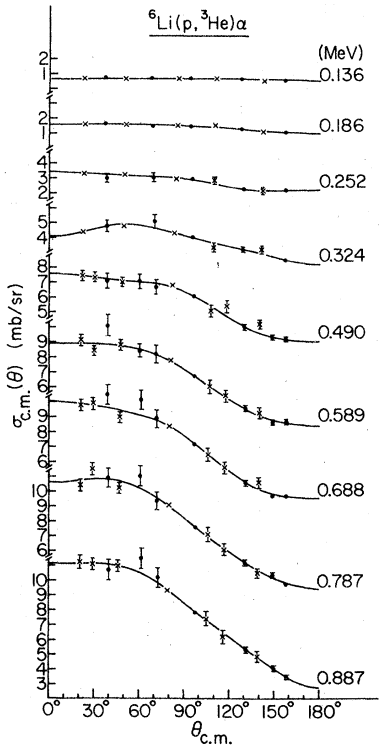

FIG. 3. Angular distributions of the ^3He particles for the $^6Li(p,^3He)$ reaction at the average proton energies indicated. The smooth curves at each energy represent the results of the Legendre polynomial fit. The points denoted by an × were obtained from the ^4He yield by use of appropriate kinematic relationships, while the solid circles were obtained from the ^3He yields. The error bars represent relative errors.

^{3}He by use of appropriate kinematic relationships, the yield of ^{3}He particles at from 10 to 14 laboratory angles was obtained. These yields were measured relative to those in the fixed monitor detector and both were corrected for small dead-time effects. Absolute differential cross sections were determined by normalization to a separately measured absolute excitation function obtained at 50° where there was no necessity to use the coincidence technique described above. In these latter measurements corrections had to be made for effective charge collection since the amount of collected charge changes with the energy of the projectile, especially at low energies (below 1 MeV). The magnitude of this correction was determined as described in Ref. 1.

The thickness of the ^{6}LiF targets was measured both by Rutherford scattering of α particles by the F in the target, and by backscattering of both α particles and protons from targets in which two thin layers of Au were sandwiched around the ^{6}LiF deposit, as discussed in Ref. 1. Thicknesses determined by both methods agreed to better than 5%. For the angular distribution measurements below 1 MeV, the LiF targets were ~25 μg/cm^2 deposits,

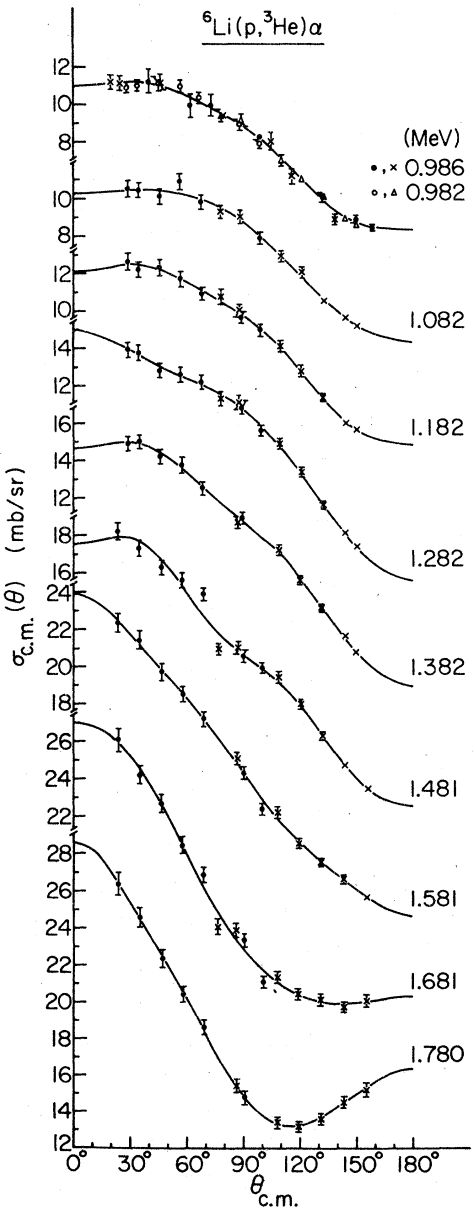

FIG. 4. Same caption as for Fig. 3.

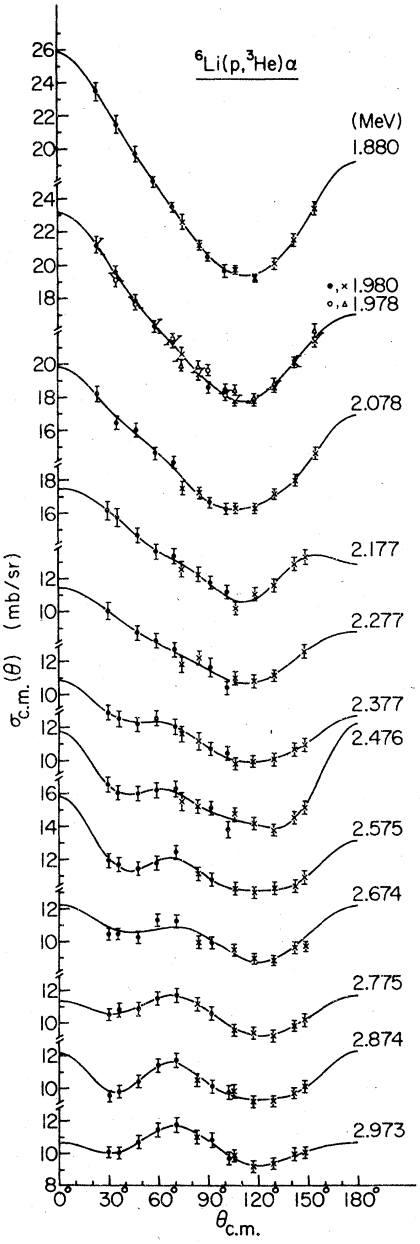

FIG. 5. Same caption as for Fig. 3.

TABLE I. Values of coefficients B_L in the expansion of the differential cross section (in the c.m. system) into a series of Legendre polynomials $[\sigma(\theta)=\sum_L B_L P_L(\cos\theta)]$.

E_p (MeV)	B_0 (mb/sr)	B_1 (mb/sr)	B_2 (mb/sr)	B_3 (mb/sr)	B_4 (mb/sr)	B_5 (mb/sr)	B_6 (mb/sr)	σ_r [a] (mb)
0.136	0.683±0.005	0.005±0.011	−0.04 ±0.01					8.58±0.21
0.186	1.45 ±0.01	0.28 ±0.03	−0.11 ±0.03					18.2 ±0.46
0.257	2.80 ±0.03	0.66 ±0.05	−0.16 ±0.05	−0.06 ±0.08	0.16 ±0.08			35.2 ±0.88
0.324	3.98 ±0.05	1.18 ±0.10	−0.51 ±0.09	−0.26 ±0.15	−0.29 ±0.15			50.0 ±1.3
0.490	5.85 ±0.06	2.34 ±0.11	−0.85 ±0.11	−0.07 ±0.19	0.34 ±0.18			73.5 ±1.8
0.589	6.79 ±0.07	3.09 ±0.12	−0.72 ±0.13	−0.36 ±0.21	0.11 ±0.20			85.3 ±2.1
0.688	7.27 ±0.08	3.55 ±0.14	−0.78 ±0.14	−0.31 ±0.23	0.325±0.22			91.3 ±2.3
0.787	7.94 ±0.08	3.98 ±0.14	−0.735±0.14	−0.40 ±0.23	−0.20 ±0.23			99.8 ±2.5
0.887	8.18 ±0.06	4.21 ±0.10	−0.90 ±0.10	−0.21 ±0.16	−0.32 ±0.19	0.18 ±0.19		102.8 ±2.6
0.986	8.18 ±0.08	4.30 ±0.14	−1.14 ±0.14	−0.10 ±0.23	0.13 ±0.27	−0.36 ±0.28		102.8 ±2.6
1.082	7.87 ±0.07	4.21 ±0.14	−1.67 ±0.17	−0.12 ±0.27	0.13 ±0.28	−0.10 ±0.33		98.9 ±2.5
1.182	8.99 ±0.05	4.92 ±0.10	−1.53 ±0.12	0.155±0.19	0.02 ±0.19	−0.44 ±0.23		113.0 ±2.8
1.282	9.73 ±0.05	5.76 ±0.11	1.77 ±0.13	0.86 ±0.20	0.00 ±0.20	0.055±0.25		122.3 ±3.1
1.382	10.21 ±0.06	6.18 ±0.11	−1.39 ±0.14	0.54 ±0.21	−0.52 ±0.22	−0.37 ±0.28		128.3 ±3.2
1.481	11.68 ±0.14	6.90 ±0.25	−0.41 ±0.33	0.88 ±0.44	1.45 ±0.66	0.41 ±0.78		146.8 ±3.7
1.581	14.52 ±0.09	7.93 ±0.16	0.57 ±0.21	0.27 ±0.27	0.15 ±0.30	0.46 ±0.35		182.5 ±4.6
1.681	16.50 ±0.15	7.66 ±0.29	3.27 ±0.38	−0.06 ±0.51	−0.13 ±0.55	−0.21 ±0.62		207.3 ±5.2
1.780	17.24 ±0.04	6.32 ±0.08	4.78 ±0.12	−0.55 ±0.13	0.19 ±0.18	0.37 ±0.19	0.28±0.20	216.6 ±5.9
1.880	15.95 ±0.05	4.38 ±0.10	5.11 ±0.15	−1.12 ±0.17	1.13 ±0.23	0.08 ±0.21	0.39±0.23	200.4 ±5
1.980	14.85 ±0.06	3.52 ±0.11	4.39 ±0.17	−0.81 ±0.20	0.82 ±0.26	0.41 ±0.25	0.02±0.29	186.6 ±4.7
2.078	13.50 ±0.09	2.34 ±0.17	3.73 ±0.26	−0.93 ±0.31	0.61 ±0.40	0.05 ±0.39	0.55±0.46	169.6 ±4.2
2.177	12.84 ±0.13	2.13 ±0.23	2.69 ±0.52	−0.65 ±0.46	0.24 ±0.73	0.83 ±0.51	−0.62±0.67	161.4 ±4
2.277	12.38 ±0.18	1.69 ±0.32	2.28 ±0.72	−0.68 ±0.60	0.57 ±1.05	0.30 ±0.68	−0.13±1.07	155.6 ±3.9
2.377	11.33 ±0.08	1.51 ±0.13	1.32 ±0.30	−0.93 ±0.26	0.69 ±0.41	0.51 ±0.29	0.46±0.39	142.4 ±3.6
2.476	11.46 ±0.14	1.06 ±0.23	1.58 ±0.51	−1.26 ±0.45	1.74 ±0.71	−0.03 ±0.52	1.24±0.67	144.0 ±3.6
2.575	11.21 ±0.10	1.09 ±0.17	1.03 ±0.36	−0.71 ±0.31	1.30 ±0.50	0.96 ±0.39	0.98±0.48	140.9 ±3.5
2.674	10.16 ±0.15	0.85 ±0.25	0.76 ±0.52	−1.27 ±0.45	1.22 ±0.73	0.43 ±0.56	0.08±0.71	127.6 ±3.2
2.775	10.51 ±0.07	0.85 ±0.11	−0.002±0.24	−1.53 ±0.21	0.76 ±0.33	0.50 ±0.26	0.22±0.32	132.0 ±3.3
2.874	10.29 ±0.09	0.61 ±0.34	0.04 ±0.34	−1.45 ±0.63	0.89 ±0.46	0.79 ±0.68	0.99±0.44	129.3 ±3.2
2.973	10.41 ±0.08	0.68 ±0.13	−0.45 ±0.31	−1.49 ±0.26	0.57 ±0.42	0.81 ±0.31	0.12±0.41	130.8 ±3.3

[a] Errors on σ_r are relative errors only.

while for the higher energy measurements thicknesses of 70–80 $\mu g/cm^2$ were used. The proton energies quoted in this report represent average values which differ from the incident energy because of (small) energy loss in the ^{6}LiF targets. Although the dissociation[11] in the target of the incident molecular ion H_3^+, which was used at energies below 0.5 MeV, introduced an additional spread in the proton energy (~7 keV for 1-MeV H_3^+), the average proton energy was not changed (to within a few eV).

The beam line and target chamber system were pumped by liquid-nitrogen trapped turbomolecular pumps and a liquid-nitrogen cooled sorption trap to typical chamber pressures of less than 10^{-6} Torr. In addition, the beam entering the chamber passed through an inline liquid-nitrogen cold finger. Because of this, and since beam currents were less than 50 nA, carbon contaminant buildup on the ^{6}LiF targets was kept to a minimum. Even so, targets were replaced frequently during the experiment particularly for runs at low incident energies where the cross section varies rapidly.

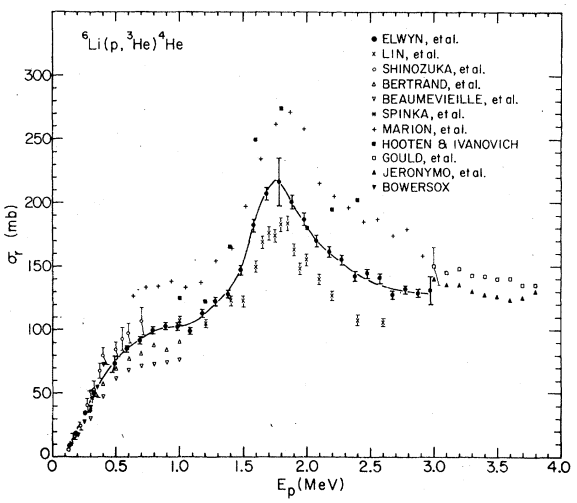

FIG. 7. Integrated cross sections ($\sigma_\gamma = 4\pi B_0$) for the ^{6}Li(p, ^{3}He) reaction, compared with previous measurements (Refs. 7, 8, 10, 13, 14). The solid line is to guide the eye. The large error bars on a few of the solid points are representative of the total uncertainty; the smaller bars indicate the relative accuracy of the measurements.

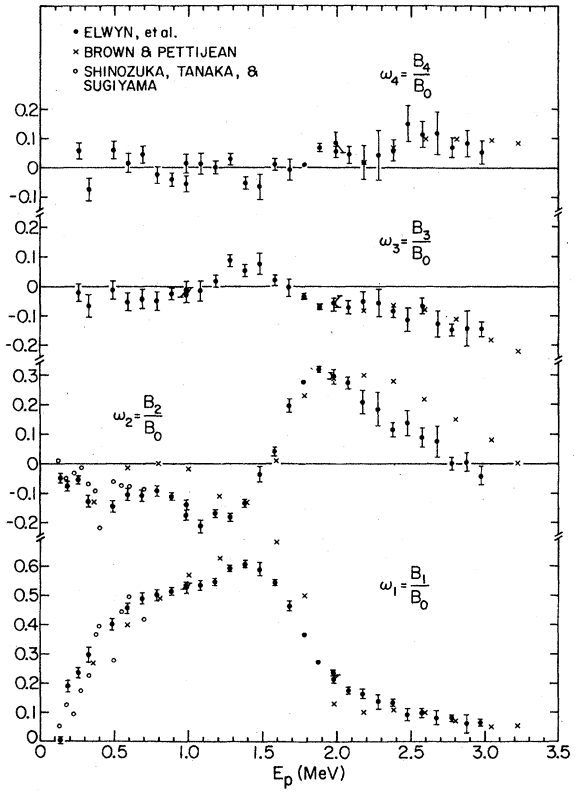

FIG. 6. Ratios of Legendre polynomial coefficients $\omega_L = B_L/B_0$ for the ^{6}Li(p, ^{3}He) reaction. Comparison with the results of Refs. 8 and 12 are shown.

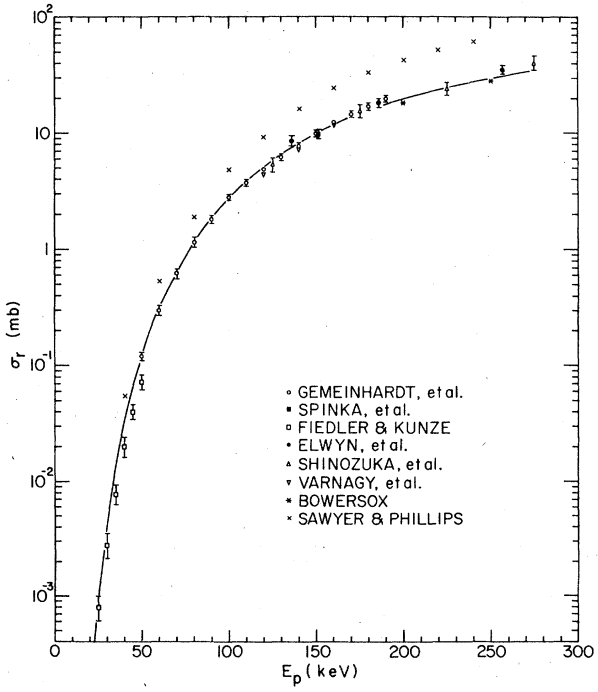

FIG. 8. Integrated cross sections ($\sigma_\gamma = 4\pi B_0$) for the ^{6}Li(p, ^{3}He) reaction at energies below 300 keV. The previous measurements are from Refs. 7, 8, 9, 10, and 17. The solid curve represents calculations based on Eq. (2.21) in Ref. 16, with $t = 188$ and $\bar{\gamma} \approx 0$, as discussed in the text.

III. RESULTS

The differential cross sections in the center-of-mass system are shown in Figs. 3–5 at each average incident-proton energy. The error bars represent the relative uncertainties which vary from about 10% at a few angles at the lowest energies to about 2% at some higher energies, and are typically 3–5%. The solid curves result from fitting the differential cross sections to a series of Legendre polynomials at each energy. The coefficients B_L in the Legendre polynomial expansion are listed in Table I. The errors associated with them are generated in the fitting program. The ratios of the coefficients are compared with previous measurements[8,12] in Fig. 6.

TABLE II. Reaction rate parameters $\langle\sigma v\rangle$ and reactivity parameters $\langle\sigma v\rangle Q$ ($Q = 4.02$ MeV) for the $^6Li(p,^3He)^4He$ reaction.

kT (MeV)	$\langle\sigma v\rangle$ ($cm^3\,sec^{-1}$)	$\langle\sigma v\rangle Q$ ($cm^3\,MeV\,sec^{-1}$)
0.001	8.826 $E-29$ [a]	3.548 $E-28$
0.002	1.183 $E-25$	4.754 $E-25$
0.003	3.740 $E-24$	1.503 $E-23$
0.004	3.244 $E-23$	1.304 $E-22$
0.005	1.504 $E-22$	6.045 $E-22$
0.006	4.913 $E-22$	1.975 $E-21$
0.007	1.290 $E-21$	5.186 $E-21$
0.008	2.889 $E-21$	1.162 $E-20$
0.009	5.692 $E-21$	2.288 $E-20$
0.01	1.008 $E-20$	4.053 $E-20$
0.02	1.802 $E-19$	7.245 $E-19$
0.03	7.116 $E-19$	2.861 $E-18$
0.04	1.753 $E-18$	7.048 $E-18$
0.05	3.280 $E-18$	1.319 $E-17$
0.06	5.201 $E-18$	2.091 $E-17$
0.07	7.421 $E-18$	2.983 $E-17$
0.08	9.865 $E-18$	3.966 $E-17$
0.09	1.247 $E-17$	5.014 $E-17$
0.1	1.520 $E-17$	6.109 $E-17$
0.2	4.454 $E-17$	1.791 $E-16$
0.3	7.475 $E-17$	3.005 $E-16$
0.4	1.040 $E-16$	4.179 $E-16$
0.5	1.304 $E-16$	5.240 $E-16$
0.6	1.532 $E-16$	6.159 $E-16$
0.7	1.726 $E-16$	6.938 $E-16$
0.8	1.888 $E-16$	7.588 $E-16$
0.9	2.022 $E-16$	8.127 $E-16$
1	2.132 $E-16$	8.572 $E-16$
2	2.557 $E-16$	1.028 $E-15$
3	2.588 $E-16$	1.040 $E-15$
4	2.579 $E-16$	1.036 $E-15$
5	2.587 $E-16$	1.039 $E-15$
6	2.614 $E-16$	1.051 $E-15$
7	2.658 $E-16$	1.063 $E-15$
8	2.713 $E-16$	1.091 $E-15$
9	2.776 $E-16$	1.116 $E-15$
10	2.844 $E-16$	1.143 $E-15$

[a] Read as 8.826×10^{-29}.

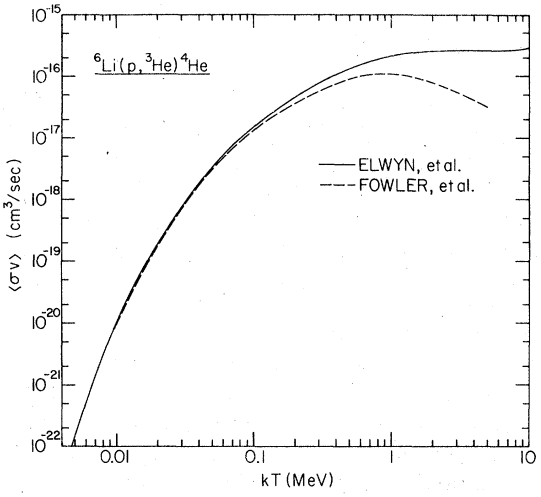

FIG. 9. Reaction rate parameters $\langle\sigma v\rangle$ as a function of kT based on the present measurements, as discussed in the text, compared to results from Ref. 18.

Integrated (reaction) cross sections ($\sigma_r = 4\pi B_0$) are shown in the last column of Table I and plotted as a function of E_p in Fig. 7. Absolute uncertainties are about 9%; the largest contribution to this value arises from the estimated error in the determination of the target thickness. The present measurements are in reasonably good agreement with the earlier measurements of Refs. 9 and 10 and the more recent results of Ref. 8 in the regions of overlap. The present results appear to be systematically lower than those of Gould *et al.*[13] in the energy region near and above 3 MeV, although apparently in agreement within the estimated absolute uncertainties.

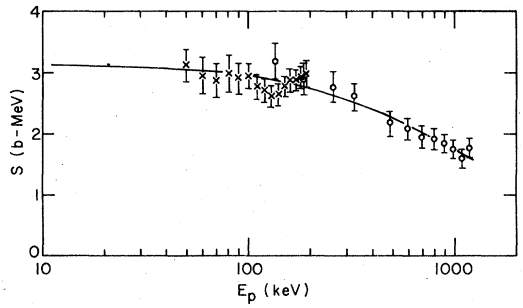

FIG. 10. Experimental astrophysical S factors based on the present measurements (open circles) and data of Ref. 9 (×'s) for proton energies up to the Coulomb barrier (~1.2 MeV for a radius $R = 3.66$ fm). The solid curve is the result of a least-squares fit to Eq. (2) in the text.

TABLE III. Summary of fits to S factor expansion coefficients [see Eq. (2) in text].

$S(0)$ (MeV b)	$S'(0)/S(0)$ (MeV^{-1})	$\frac{1}{2}S''(0)/S(0)$ (MeV^{-2})	c.m. energy range (MeV)	Reference and remarks
3.14	−0.79	0.32	0.04 − 1.0	Present and Ref. 9
3.145	−0.70	0.06	0.001 − 0.5	Present, Ref. 9, and extrapolation (see Fig. 8 and Sec. IV A)
2.4	−0.8	0.42	0.02 − 1.0	Ref. 23
3.352	−0.522	−0.191	10^{-5} − 1.0	Ref. 24

IV. DISCUSSION

A. Thermonuclear reaction rates

There have been a number of proposals[6] for advanced fusion fuels that involve the ^{6}Li(p,^{3}He)^{4}He reaction either by itself or, perhaps more promising, in a completely "catalyzed" mode. In this latter situation the ^{3}He formed in the primary ^{6}Li+p process reacts in one branch with the ^{6}Li fuel itself through the ^{6}Li(^{3}He,p)2^{4}He reaction to regenerate the proton which may then interact again with the ^{6}Li; the whole cycle (including any other branch processes) operates in a manner similar to a chain reaction.[6] The feasibility of these proposals depends in part on the reaction rates for the various processes taking part in the chain.

We have calculated reaction rate parameters $\langle\sigma v\rangle$ for the ^{6}Li(p,^{3}He) reaction (where σ is the reaction cross section σ_r, v is the relative velocity between the interacting nuclei in the incident channel, and the average is taken over a Maxwell-Boltzmann distribution of velocities) by the method discussed by Elwyn *et al.*[15] In this analysis we used reaction cross section data given by Gemeinhardt *et al.*[9] for energies between 50 and 100 keV, the values listed in Table I for proton energies between 0.1 and 3.0 MeV, and those given by Gould *et al.*[13] for the energy range 3 to 10 MeV. For energies below 50 keV, cross sections down to 1 eV were obtained from an extrapolation formula given by Monahan *et al.*[16] The expression [Eq. (2.21) in Ref. 16] involves two adjustable parameters which were determined to be $t=188$ and $\bar{\gamma}\approx 0$ from a least-squares fit to the data of Gemeinhardt *et al.*[9] below 90 keV. The solid curve in Fig. 8 is the result of this calculation. Also shown are various cross section measurements,[7-10,17] taken at low energies, which were not included in the least-squares fit.

Values of $\langle\sigma v\rangle$ and the reactivity parameter $\langle\sigma v\rangle Q$ [where $Q=4.02$ MeV, the Q value for the ^{6}Li(p,^{3}He) reaction] are listed in Table II, and $\langle\sigma v\rangle$ is plotted as a function of kT in Fig. 9. The reaction rates are observed to be somewhat larger (at least for $kT \geq 100$ keV) than those based on the

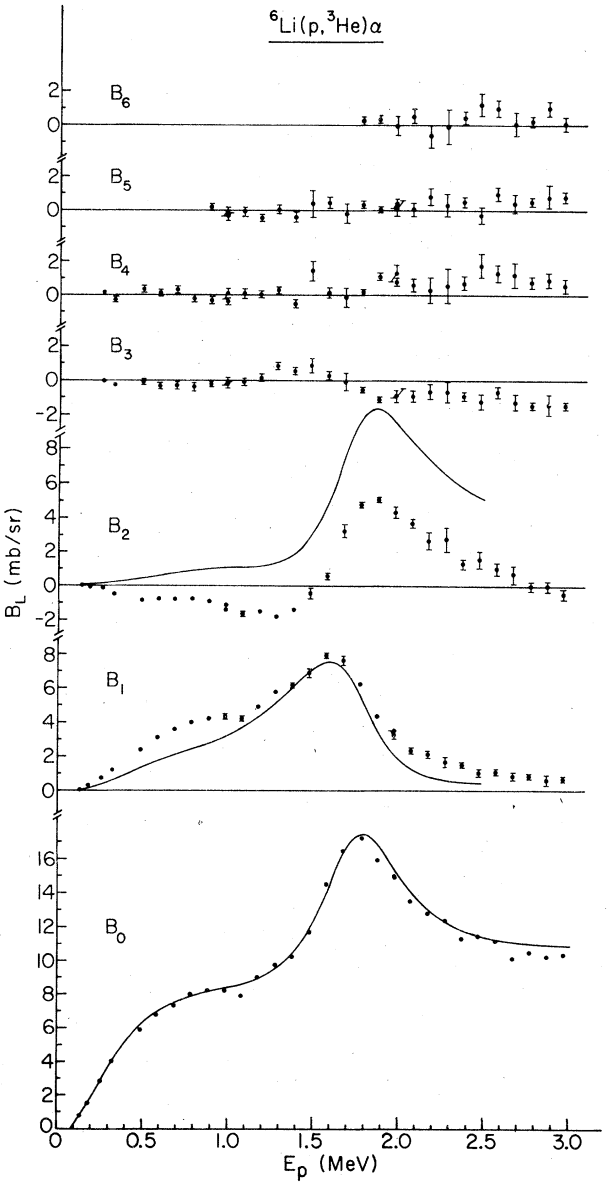

FIG. 11. The coefficients B_L from the Legendre polynomial analysis of the measured angular distributions compared to the preliminary calculations (smooth curves), which include only $l=0$ and $l=1$ partial waves, of Dodder and Hale (Refs. 5 and 26).

formula given by Fowler *et al.*[18] The results recently published in Ruby and Lung[19] are about 25% greater than the present values for 100 keV $\leq kT \leq 1$ MeV.

B. Astrophysical S factor

Rates for the destruction, or burning, of ^{6}Li are also important in several areas of astrophysics. In many of these applications it is customary[20] to parameterize the reaction cross section in terms of the astrophysical S factor defined, for energies well below the Coulomb barrier, by the expression[21]

$$\sigma_r = \frac{S}{E}\exp(-2\pi\eta). \tag{1}$$

Here $2\pi\eta = 2\pi Z_1 Z_2 e^2/\hbar v = 0.9931 Z_1 Z_2 M^{1/2}/E^{1/2}$, where E is the center-of-mass energy in MeV and M is the reduced mass. Experimental S factors based on the present measurements for the ^{6}Li$(p,^3$He) reaction are plotted in Fig. 10 as a function of (lab) proton energy E_p for energies up to the Coulomb barrier. The solid curve represents a best fit to the second-order Maclaurin series

$$S(E) = S(0)\{1 + [S'(0)/S(0)]E + \tfrac{1}{2}[S''(0)/S(0)]E^2\}, \tag{2}$$

with the parameters[22] $S(0)$, $S'(0)/S(0)$, and $\frac{1}{2}S''(0)/S(0)$ given in the first line of Table III. The second line in this table lists the values obtained when extrapolated cross sections (see Fig. 8) between 1 and 40 keV are included with the present data and those of Ref. 9. Also shown are the results of Audouze and Reeves[23] from an analysis of earlier measurements, and values obtained recently by Baker *et al.*[24] from a multichannel R-matrix fit to data on the ^{7}Be compound system. As seen in the table (as well as in further calculations), the value of the coefficient of the term quadratic in E is quite sensitive to the energy range of the cross sections used in the analyses.

C. Cross section calculations

The most recent compilation[25] of the properties of light nuclei displays the correspondence between the energy levels of the mirror pair ^{7}Li and ^{7}Be up to an excitation energy of about 10 MeV. Using this correspondence, Dodder and Hale[5] have applied approximate isospin conservation in a multilevel, multichannel R-matrix analysis of mass-7 compound systems to predict the cross sections for the ^{6}Li$(p,^3$He$)^4$He reaction. Preliminary calculations[26] which include *only* $l=0$ and $l=1$ partial waves in the p-^{6}Li channel are shown in Fig. 11. The experimental points are the Legendre polynomial coefficients from Table I. The relatively poor agreement between calculated and experimental B_1 and B_2 coefficients, coupled with small experimental B_3 and B_4 values and the observed excellent reproduction of the measured integrated cross sections (i.e., B_0 coefficients), suggest that $l=2$ partial waves, neglected in this preliminary analysis, are important primarily through interference with the major $l=0$ and $l=1$ contributions. More detailed calculations[27] are currently in progress.

ACKNOWLEDGMENTS

It is a pleasure to acknowledge useful discussions with Dr. J. E. Monahan. We would also like to thank R. Amrein and the operating staff of the Dynamitron accelerator for their cooperation in performing the measurements reported here.

[1] A. J. Elwyn, R. E. Holland, C. N. Davids, L. Meyer-Schützmeister, J. E. Monahan, F. P. Mooring, and W. Ray, Jr., Phys. Rev. C 16, 1744 (1977).

[2] R. E. Holland, A. J. Elwyn, C. N. Davids, F. J. Lynch, L. Meyer-Schützmeister, J. E. Monahan, F. P. Mooring, and W. Ray, Jr., Phys. Rev. C 19, 592 (1979).

[3] A preliminary report of this work for proton energies up to 1 MeV is given by A. J. Elwyn, R. E. Holland, C. N. Davids, L. Meyer-Schützmeister, F. P. Mooring, and W. Ray, Jr., Bull. Am. Phys. Soc. 23, 97 (1978).

[4] G. M. Hale, in *Proceedings of the Conference on Cross Sections and Technology*, NBS Special Publication No. 425 (National Bureau of Standards, Washington, D. C., 1975), Vol. 1, p. 302; G. M. Hale, in *Proceedings of a Conference on Nuclear Theory in Neutron Nuclear Data Evaluation*, IAEA-190 (International Atomic Energy Agency, Vienna, 1976), Vol. II, p. 1.

[5] D. C. Dodder and G. M. Hale, in *Proceedings of an International Conference on Neutron Physics and Nuclear Data for Reactors and Other Applied Purposes*, Harwell, U. K., 1978 (OCDE Nuclear Energy Agency, Paris, 1978), p. 490.

[6] See, e.g., a number of articles, in *Proceedings of the Review Meeting on Advanced-Fuel Fusion*, EPRI ER-536-SR (Electric Power Research Institute, Palo Alto, Calif., 1977); J. R. McNally, Nucl. Fusion 11, 187 (1971); J. R. McNally, in Proceedings of the 1979 IEEE International Conference on Plasma Science, Quebec, 1979 (to be published).

[7] R. B. Bowersox, Phys. Rev. 55, 323 (1939); G. A. Sawyer and J. A. Phillips, Los Alamos Scientific Laboratory Report No. LA-1578, 1953 (unpublished); J. B. Marion, G. Weber, and F. S. Mozer, Phys. Rev. 104, 1402 (1956); B. W. Hooten and M. Ivanovich, AERE Harwell Report No. AERE-PR/NP18, 1972 (unpub-

lished); F. Bertrand, G. Grenier, and J. Pornet, Centre d'Etudes de Limeil Rapport No. CEA-R-3428, 1968 (unpublished); H. Beaumevieille, J. P. Longequeue, N. Longequeue, and R. Bouchez, J. de Physique 25, 933 (1964); C. S. Lin, W. S. Hou, M. Wen, and J. C. Chen, Nucl. Phys. A275, 93 (1977).

[8]T. Shinozuka, K. Tanaka, and K. Sugiyama, Nucl. Phys. A326, 47 (1979); private communication.

[9]W. Gemeinhardt, D. Kamke, and C. Von Rhöneck, Zeit. für Physik 197, 58 (1966).

[10]H. Spinka, T. Tombrello, and H. Winkler, Nucl. Phys. A164, 1 (1971).

[11]M. J. Gaillard, D. S. Gemmell, G. Goldring, I. Levine, W. J. Pietsch, J. C. Poizat, A. J. Ratkowski, J. Remillieux, Z. Vager, and B. J. Zabransky, Phys. Rev. A 17, 1797 (1978).

[12]L. Brown and C. Pettijean, Nucl. Phys. A117, 343 (1968).

[13]C. R. Gould, R. O. Nelson, J. R. Williams, and J. R. Boyce, Nucl. Sci. Eng. 55, 267 (1974).

[14]J. M. F. Jeronymo, G. S. Mani, and A. Sadeghi, Nucl. Phys. 43, 424 (1963).

[15]A. J. Elwyn, J. E. Monahan, and F. J. D. Serduke, Nucl. Sci. Eng. 63, 343 (1977).

[16]J. E. Monahan, A. J. Elwyn, and F. J. D. Serduke, Nucl. Phys. A269, 61 (1976).

[17]M. Varnagy, J. Csikai, J. Szabo, S. Szegedi, and J. Banhalmi, Nucl. Instrum. Methods 119, 451 (1974); O. Fiedler and P. Kunze, Nucl. Phys. A96, 513 (1967).

[18]W. A. Fowler, G. R. Caughlan, and B. A. Zimmermann, Ann. Rev. Astron. Astrophys. 13, 69 (1975).

[19]L. Ruby and T.-P. Lung, Nucl. Sci. Eng. 69, 107 (1979).

[20]See, for example, D. D. Clayton, *Principles of Stellar Evolution and Nucleosynthesis* (McGraw-Hill, New York, 1968), Chap. 4.

[21]This extrapolation formula is an approximation to the more rigorous expression used above (Sec. IV A) and derived in Ref. 16. In Eq. (1), the exact Coulomb penetrability is approximated by the Gamow form [exp $(-2\pi\eta)$], the validity of which is discussed by, for example, Monahan *et al.* (Ref. 16) and Clayton (Ref. 20). For the situation discussed in Sec. IV A, in which the parameter $\bar{\gamma}$ in Eq. (2.21) of Ref. 16 is approximately equal to zero, the ratio of the t parameter [in Eq. (2.21)] to the S factor [in Eq. (1) in the text] should be constant provided that the exact Coulomb penetrability has the same dependence on energy as the form $\exp(-2\pi\eta)$. This is the case at energies well below the Coulomb barrier.

[22]Spinka *et al.* (Ref. 10) define a slightly different S factor $\tilde{S}$, by $\tilde{S} = Se^{gE}$, where $g = 0.122\ (MR^3/Z_1Z_2)^{1/2}$, S is defined by Eq. (1), and R is the nuclear radius parameter (see also Ref. 20). When S values are calculated for $R = 3.66$ fm (Ref. 10) and then fit to an expression similar to Eq. (2), we find $\tilde{S}(0) = 3.17$ MeV b, $\tilde{S}'(0)/\tilde{S}(0) = -0.43\,\mathrm{MeV}^{-1}$, and $\frac{1}{2}\tilde{S}''(0)/\tilde{S}(0) = 0.26\ \mathrm{MeV}^{-2}$.

[23]J. Audouze and H. Reeves, Astrophys. J. 158, 419 (1969).

[24]S. D. Baker, E. K. Biegert, D. C. Dodder, and G. M. Hale (unpublished).

[25]F. Ajzenberg-Selove, Nucl. Phys. A320, 1 (1979).

[26]G. M. Hale, private communication. We would like to thank Dr. Hale for providing these preliminary calculations for inclusion in this report.

[27]D. C. Dodder, G. M. Hale, S. D. Baker, and E. K. Biegert (unpublished).